JTTEE5 6:181-186


# Thick Thermal Barrier Coatings for Diesel Engines

*M.B. Beardsley*

**The Caterpillar approach to applying thick thermal barrier coatings (TTBC) to diesel engine combustion chambers has been to use advanced modeling techniques to predict engine conditions and combine this information with fundamental property evaluation of TTBC systems to predict engine performance and TTBC stress states. Engine testing has been used to verify the predicted performance of the TTBC systems and to provide information on failure mechanisms.**

**The objective of the Caterpillar program has been to advance the fundamental understanding of thick thermal barrier coating systems. Areas of TTBC technology examined in this program include powder characteristics and chemistry; bond coat composition; coating design, microstructure, and thickness effects on properties, durability, and reliability; and TTBC "aging" effects (microstructural and property changes) under simulated diesel engine operating conditions. Methods to evaluate the reliability and durability of TTBCs have been developed to understand the fundamental strength of TTBCs for particular stress states.**

**Keywords** diesel engine, durability, mechanical properties, reliability, thermal barriers

## 1. Introduction

PREVIOUS REVIEWS of thermal barrier coating technology concluded that the current level of understanding of coating system behavior is inadequate, and the lack of fundamental understanding may impede the application of TTBCs to diesel engines (Ref 1).

Fifteen thick thermal barrier coating (TTBC) ceramic powders were evaluated. These powders were selected to investigate the effects of different chemistries, different manufacturing methods, lot-to-lot variations, different suppliers, and varying impurity levels (Table 1 [Ref 2]). Results of powder characterization for chemistry, particle size distribution, surface area, crystallographic phases, apparent density, and Hall flow are given in Tables 2 to 6. The chemical analysis found that the three spray-dried and sintered materials used in the impurity study (lots G, N, and O) range from low levels of alumina and silica (N), low alumina and mid-level silica (G), to high alumina and silica (O) (Table 2). The chemistries of the powders produced by different manufacturing methods (HOSP proprietary Metco process, spray-dried, spray-dried and sintered, fused and crushed, and solgel materials) also show slightly different ranges of impurities reflecting the different manufacturing methods.

Particle size distributions, as measured by the laser light scattering method of the 15 materials, showed small variations in the mean and size ranges (Table 3). The surface areas of the powders show a wide range, even for similarly manufactured powders (lots G, N, and O and lots A, L, and M [Table 4]). The crystallographic phases were as expected for the powder processing methods investigated (Table 5). The Hall flow and apparent density of the materials did not have significant meaning to the results, particularly the Hall flow, which indicated flow problems with several powders that did not occur in use (Table 6).

**M.B. Beardsley,** Caterpillar Inc., Peoria, IL 61656-1875, USA.

## 2. Spray Processing and Thermal Conductivity

Fifteen materials were sprayed using 36 parameters selected by a design of experiments to determine the effects of primary gas (argon and $N_2$), primary gas flow rate, voltage, arc current, powder feed rate, carrier gas flow rate, and spraying distance.

**Table 1 Powders selected for evaluation to investigate the effects of different chemistries, different manufacturing methods, lot-to-lot variations, different suppliers, and varying impurity levels**

| Material | Mfg method | Supplier | Lot |
|---|---|---|---|
| 8% yttria-zirconia | HOSP(a) | Metco | A |
| 20% yttria-zirconia | spray dried | Metco | B |
| 24% ceria-zirconia | HOSP(a) | Metco | C |
| calcium titanate | spray dried | Metco | D |
| mullite | fused and crushed | Metco | E |
| **Different manufacturing methods** | | | |
| 8% yttria-zirconia | sprayed dried | Metco | F |
| 8% yttria-zirconia | spray dried and sintered | Metco | G |
| 8% yttria-zirconia | fused and crushed | Norton | H |
| 8% yttria-zirconia | sol gel | Metco | I |
| **Different Suppliers** | | | |
| 8% yttria-zirconia | sprayed/compacted/sintered | Zircoa | J |
| 8% yttria-zirconia | spray dried and sintered | Met Tech | K |
| **Lot-to-lot variations** | | | |
| 8% yttria-zirconia | HOSP(a) | Metco | L |
| 8% yttria-zirconia | HOSP(a) | Metco | M |
| **Impurities** | | | |
| 8% yttria-zirconia | spray dried and sintered | Metco | N |
| 8% yttria-zirconia | spray dried and sintered | Metco | O |

(a) HOSP is a proprietary Metco manufacturing method.

**Table 2 Chemistries of the 15 selected materials**

| Material | Lot ID | $Al_2O_3$ | CaO | $Fe_2O_3$ | $HfO_2$ | MgO | $SiO_2$ | $TiO_2$ | Th+U | $Y_2O_3$ | $CeO_2$ | $ZrO_2$ | $Na_2O$ |
|---|---|---|---|---|---|---|---|---|---|---|---|---|---|
| 8% YSZ-HOSP | A | <0.01 | <0.01 | <0.01 | 1.73 | <0.01 | <0.01 | 0.09 | <0.01 | 7.98 | <0.01 | 90.21 | 0.27 |
| 20% YSZ-S/D | B | 0.06 | 0.03 | <0.01 | 1.51 | <0.01 | 0.16 | 0.07 | 0.03 | 19.34 | <0.01 | 77.4 | 0.08 |
| 24% CSZ-HOSP | C | <0.01 | 0.07 | 0.02 | 1.27 | 0.04 | 0.04 | 0.08 | <0.01 | 2.42 | 25.12 | 70.84 | 0.15 |
| $CaTiO_5$ | D | 0.21 | 40.9 | 0.06 | | 0.23 | 0.43 | 57.54 | <0.01 | <0.01 | <0.01 | 0.09 | 0.18 |
| mullite | E | 74.34 | 0.03 | 0.01 | | <0.01 | 25.32 | <0.01 | <0.01 | <0.01 | <0.01 | 0.01 | 0.37 |
| 8% YSZ-S/D | F | 0.27 | 0.13 | 0.06 | 1.79 | <0.01 | 0.72 | 0.1 | 0.05 | 7.34 | <0.01 | 89.44 | 0.1 |
| 8% YSZ-S/D-S | G | 0.01 | 0.01 | 0.01 | 1.74 | <0.01 | 0.18 | 0.04 | <0.01 | 7.8 | <0.01 | 90.21 | 0.29 |
| 8% YSZ-F/C | H | 0.03 | 0.04 | <0.01 | 1.64 | <0.01 | <0.01 | 0.2 | <0.01 | 7.46 | <0.01 | 90.63 | 0.08 |
| 8% YSZ-solgel | I | <0.01 | <0.01 | <0.01 | 1.58 | <0.01 | <0.01 | 0.06 | <0.01 | 7.37 | <0.01 | 90.99 | 0.18 |
| 8% YSZ-S/C-S | J | 0.08 | 0.18 | 0.11 | 1.81 | <0.01 | <0.01 | <0.01 | 0.04 | 7.5 | <0.01 | 90.28 | 0.03 |
| 8% YSZ-S/D-S | K | 0.01 | <0.01 | 0.02 | 1.84 | <0.01 | 0.22 | 0.08 | 0.01 | 7.47 | 0.01 | 90.35 | 0.16 |
| 8% YSZ-HOSP | L | <0.01 | <0.01 | 0.04 | 1.67 | <0.01 | <0.01 | 0.1 | <0.01 | 7.77 | <0.01 | 90.42 | 0.11 |
| 8% YSZ-HOSP | M | <0.01 | <0.01 | <0.01 | 1.63 | 0.03 | 0.03 | 0.13 | <0.01 | 7.58 | <0.01 | 90.51 | 0.22 |
| 8% YSZ-S/D-S | N | <0.01 | <0.01 | 0.03 | 1.65 | <0.01 | <0.01 | 0.14 | <0.01 | 7.2 | <0.01 | 90.98 | 0.22 |
| 8% YSZ-S/D-S | O | 0.26 | 0.13 | 0.05 | 1.76 | <0.01 | 0.69 | 0.1 | 0.01 | 7.01 | 0.01 | 89.99 | 0.24 |

HOSP, proprietary Metco manfuacturing method; S/D, spray-dried; S/D-S, spray-dried and sintered; F/C, fused and crushed; and SOLGEL, sol gel

**Table 3 Particle size distribution and mean particle size of the 15 selected materials**

| Material | Lot | Size, μm | | | Mean size, μm |
|---|---|---|---|---|---|
| | | 10% | 50% | 90% | |
| 8% YSZ-HOSP | A | 20.37 | 50.87 | 103.78 | 56.76 |
| 20% YSZ-S/D | B | 30.16 | 66.36 | 124.11 | 74.15 |
| 24% CSZ-HOSP | C | 22.12 | 50.92 | 103.15 | 56.92 |
| $CaTiO_5$ | D | 39.23 | 67.09 | 119.88 | 75.61 |
| mullite | E | 52.32 | 94.38 | 147.48 | 96.22 |
| 8% YSZ-S/D | F | 29.41 | 60.67 | 113.99 | 67 |
| 8% YSZ-S/D-S | G | 27.95 | 56.54 | 108.7 | 62.82 |
| 8% YSZ-F/C | H | 32.07 | 64.08 | 117.48 | 70.01 |
| 8% YSZ-solgel | I | 33.62 | 57.22 | 101.93 | 62.59 |
| 8% YSZ-S/C-S | J | 34.74 | 63.82 | 110.45 | 68.3 |
| 8% YSZ-S/D-S | K | 29.01 | 54.95 | 102.47 | 60.42 |
| 8% YSZ-HOSP | L | 25.23 | 54.08 | 105.31 | 59.9 |
| 8% YSZ-HOSP | M | 22.85 | 49.65 | 102.46 | 56.32 |
| 8% YSZ-S/D-S | N | 26.08 | 53.84 | 104.87 | 59.91 |
| 8% YSZ-S/D-S | O | 26.5 | 55.08 | 104.66 | 60.67 |

Specimens are identified in Table 2.

**Table 4 Surface areas of the 15 selected materials**

| Material | Lot | Single point, $m^2/g$ | BET, $m^2/g$ |
|---|---|---|---|
| 8% YSZ-HOSP | A | 0.3346 | 0.3461 |
| 20% YSZ-S/D | B | 1.9386 | 2.0047 |
| 24% CSZ-HOSP | C | 0.2994 | 0.3031 |
| $CaTiO_5$ | D | 2.2343 | 2.3069 |
| mullite | E | 0.1833 | 0.1440 |
| 8% YSZ-S/D | F | 3.6373 | 3.7554 |
| 8% YSZ-S/D-S | G | 1.0337 | 1.0640 |
| 8% YSZ-F/C | H | 0.0623 | 0.0442 |
| 8% YSZ-solgel | I | 4.1542 | 4.2505 |
| 8% YSZ-S/C-S | J | 0.1715 | 0.1307 |
| 8% YSZ-S/D-S | K | 0.3071 | 0.3155 |
| 8% YSZ-HOSP | L | 0.2559 | 0.2664 |
| 8% YSZ-HOSP | M | 0.2671 | 0.2790 |
| 8% YSZ-S/D-S | N | 0.7742 | 0.7970 |
| 8% YSZ-S/D-S | O | 0.2544 | 0.2706 |

Specimens are identified in Table 2.

The deposition efficiency, density, and thermal conductivity of the resulting coatings were measured. A coating with high deposition efficiency and low thermal conductivity is desired from an economic standpoint. A general trend for all 15 materials was increasing thermal conductivity with higher deposition efficiency as shown in Fig. 1. Thermal conductivity was measured by the flash diffusivity method and then calculated from the density (measured by mercury intrusion porosimeter), and the specific heat of the material. An optimum combination of thermal conductivity and deposition efficiency was found for each powder lot in follow-up experiments, and deposition parameters were chosen for full characterization.

Resulting thermal conductivity and deposition efficiency for each of the powders sprayed with optimized parameters were determined and are compared to the baseline coating (lot A, 8% yttria-zirconia, HOSP) in Fig. 2. Several of the powders exhibit lower thermal conductivity than the baseline coating with the 20% yttria-zirconia (lot B) and spray dried 8% yttria-zirconia (lot F) showing both lower thermal conductivity and higher deposition efficiency. The higher thermal conductivity of materials such as the calcium titanate (lot B) may be balanced by higher deposition efficiency to achieve coatings with equivalent thermal conductance and cost. A component design question is whether higher deposition efficiency balances higher thermal

Table 5 Crystallographic phases for the 15 powders selected

| Material | Lot | Stabilized phases and tetragonal zirconia | Monoclinic zirconia | Yttria |
|---|---|---|---|---|
| 8% YSZ-HOSP | A | 91.1 | 8.9 | ND |
| 20% YSZ-S/D | B | ... | 82-80 | 18-20 |
| 24% CSZ-HOSP | C | 93.8 | 6.2 | ND |
| $CaTiO_5$ | D | 100% calcium titanate | ... | ... |
| mullite | E | 100% mullite | ... | ... |
| 8% YSZ-S/D | F | ... | 92-93 | 7-8 |
| 8% YSZ-S/D-S | G | 63.5 | 36.5 | ND |
| 8% YSZ-F/C | H | 100 | ND | ND |
| 8% YSZ-solgel | I | 100 | 0 | ND |
| 8% YSZ-S/C-S | J | 85.7 | 14.3 | ND |
| 8% YSZ-S/D-S | K | 62.5 | 37.5 | ND |
| 8% YSZ-HOSP | L | 93.0 | 7.0 | ND |
| 8% YSZ-HOSP | M | 91.1 | 8.9 | ND |
| 8% YSZ-S/D-S | N | 73.5 | 26.5 | ND |
| 8% YSZ-S/D-S | O | 70.1 | 29.9 | ND |

Specimens are identified in Table 2. ~O is not detected.

conductivity (which results in needing a thicker coating to achieve similar thermal conductance).

## 3. Strength Testing

Room temperature strengths of the optimized coatings were determined using four-point bending specimens with a 20 by 40 mm test fixture. Tensile strength was determined using free standing coatings with approximate dimensions of 1 by 10 by 50 mm, made by spraying mild steel substrates that were subsequently removed by chemical etching. Compressive strengths of the coatings were determined using composite specimens of ceramic with a bond coating on stainless steel substrates, tested with the coating in compression and the steel in tension. Dimensions of the compressive specimen were 10 by 50 mm, with a 2 mm thick substrate and 0.5 mm thick ceramic. Compressive strength of the coating was determined from an elastic bi-material analysis of the resulting failure of the coating. Coatings were tested with an as-sprayed surface. Strengths of the coatings compared to the baseline coating are shown in Fig. 3.

Although initial results show comparison of the materials appears to be straight forward, aging tests of the materials are necessary to ensure that trends in properties remain after long-term exposure to a diesel environment. Comparisons can be made, such as the comparison between lot-to-lot variations.

The three lots of 8% yttria-zirconia HOSP materials (lots A, L, M) have similar thermal conductivity, deposition efficiency, and strengths for the selected parameters (all three lots were sprayed with the same parameters). To achieve this, the parameters were selected for robustness; that is, the deposition efficiency and thermal conductivity for each lot were similar for the same parameter set. The three lots of material were sprayed with three sets of parameters, and the thermal conductivity and deposition efficiency were measured. In two of the three sets, the deposition efficiency of lots M and L was approximately one-third of the deposition efficiency of the baseline material (lot A). Spray parameters for any given chemistry and specified particle size should be chosen based on the robustness of the parameters, covering a range of lots, rather than on the results from one or two lots.

Table 6 Hall flow and apparent density for the 15 selected materials

| Material | Lot | Hall flow, s | Apparent density, $g/cm^3$ |
|---|---|---|---|
| 8% YSZ-HOSP | A | 77.9 | 2.27 |
| 20% YSZ-S/D | B | 47.3 | 1.52 |
| 24% CSZ-HOSP | C | 34.1 | 2.4 |
| $CaTiO_5$ | D | 117.4 | 1.05 |
| mullite | E | 71.6 | 1.16 |
| 8% YSZ-S/D | F | 52.2 | 1.44 |
| 8% YSZ-S/D-S | G | (a) | 1.1 |
| 8% YSZ-F/C | H | 45.1 | 2.55 |
| 8% YSZ-solgel | I | 39.2 | 1.72 |
| 8% YSZ-S/C-S | J | (a) | 1.84 |
| 8% YSZ-S/D-S | K | 40.3 | 2 |
| 8% YSZ-HOSP | L | 51.3 | 2.27 |
| 8% YSZ-HOSP | M | 81.7 | 2.26 |
| 8% YSZ-S/D-S | N | (a) | 2.26 |
| 8% YSZ-S/D-S | O | 46.3 | 1.76 |

Specimens are identified in Table 2. (a) Material did not flow.

## 4. Fatigue Testing

An axial fatigue test to determine the high cycle fatigue behavior of TTBCs was developed at the University of Illinois (Ref 4). A fatigue test apparatus was designed, and initial test work was performed that demonstrates the ability to provide a routine method of axial testing of coatings. The test fixture replaces the normal load frame and fixtures used to transmit hydraulic oil loading to the sample with the TTBC specimen.

The TTBC specimen is a composite metal/coating with stainless steel ends (Fig. 4). The coating is sprayed onto a mild steel center tube section onto stainless steel ends that are press fit. The

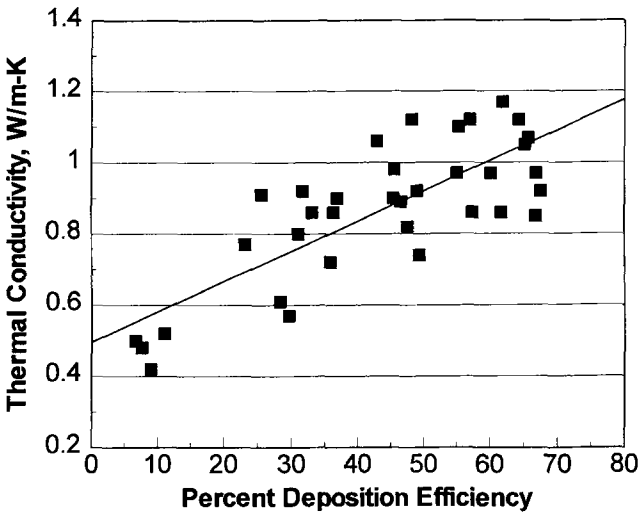


**Fig. 1** Thermal conductivity versus deposition efficiency for the 36 spray parameters used to spray the baseline 8% yttria-zirconia (HOSP, lot A)

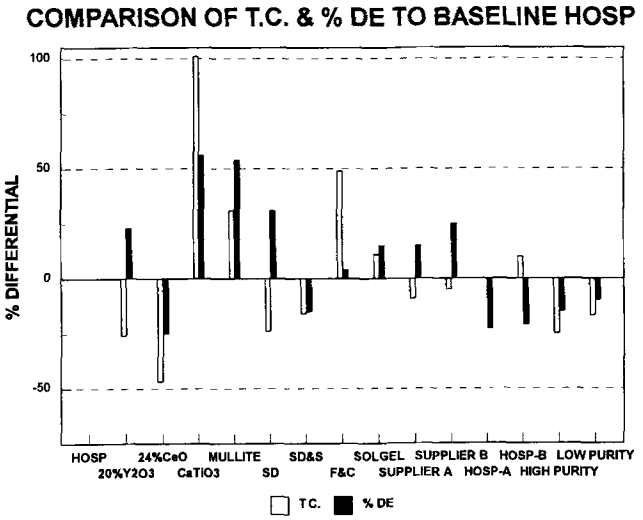


**Fig. 2** Optimized thermal conductivity (TC) and deposition efficiency (% DE) for each material, compared to the 8% yttria-zirconia baseline (HOSP, lot A)

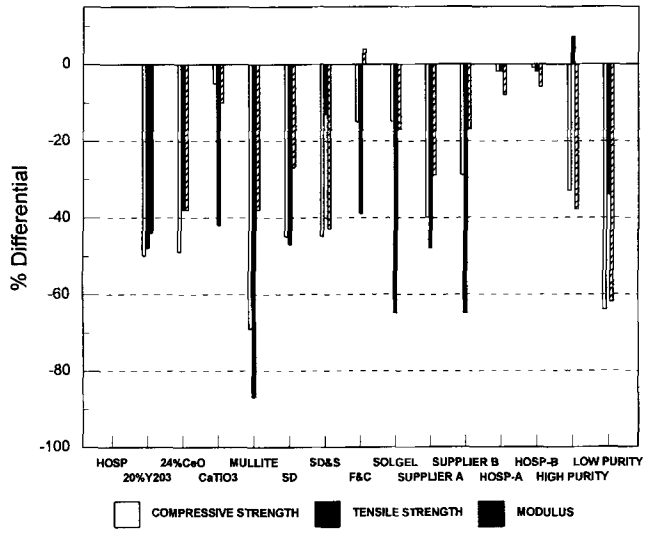


**Fig. 3** Tensile and compressive strengths and compressive elastic modulus of the 15 materials compared to the baseline 8% yttria-zirconia (HOSP, lot A)

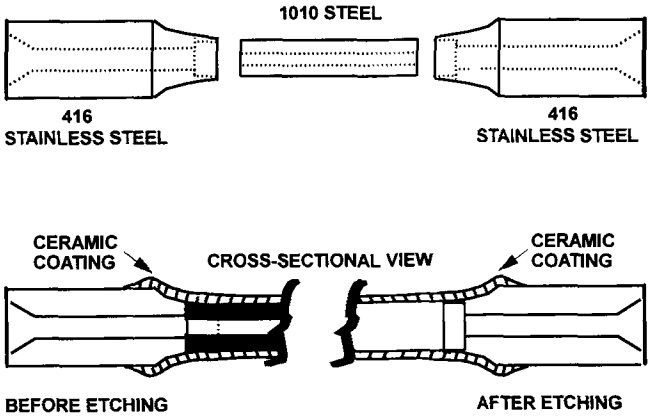


**Fig. 4** Composite metal/coating specimen used to obtain axial fatigue strength of selected coating materials

specimen is then machined. After machining, the specimen is placed in an acid bath that etches the mild steel away, leaving the TTBC attached to the stainless steel ends. Plugs are then installed in the ends, and the composite specimen is loaded in the test fixture, where the hydraulic oil pressurizes each end to apply the load. Since oil transmits the load, bending loads are minimized. This test fixture was modified to allow piston ends to be attached to the specimen, which allows tensile and compressive loading of the specimen.

A TTBC coating previously tested at room temperature, in compression using this method, resulted in stress-life data shown in Fig. 5. This data matches previous fatigue data for material obtained in four-point bending (Ref 3). Tensile data for this coating was also generated using the modified axial test fixture, resulting in stress-life data as shown in Fig. 6.

In addition to the room temperature data, specimens were recently tested at 800 °C with surprising results. At high temperature, the TTBC exhibits much higher fatigue strength (Fig. 7). This behavior is thought to be caused by sintering of the splat structure of the TTBC at the high temperature (Ref 4).

Testing of the TTBC using tension/compression cycling was conducted using the modified test fixture. The goal was to investigate the failure mechanisms of the coating and to determine if tensile and compressive fatigue damage would interact to influence the resulting coating life. Coating samples were run with various mean compressive loads and constant tensile loading, approximately equal to 90% of the tensile strength of the coating. As shown in Fig. 8, there is no interaction between the tensile and compressive load. The material fails in tension at the predicted tensile curve life. This indicates that there are two different failure mechanisms for the TTBC in tension and compression.

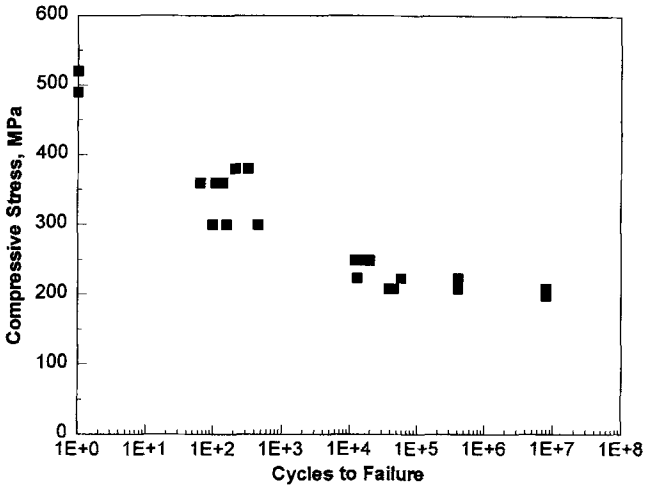


**Fig. 5** Compressive fatigue strength of an 8% yttria-zirconia TTBC at room temperature, determined using the composite metal/ceramic axial test specimen ([Ref 4] stress ratio=0.07)

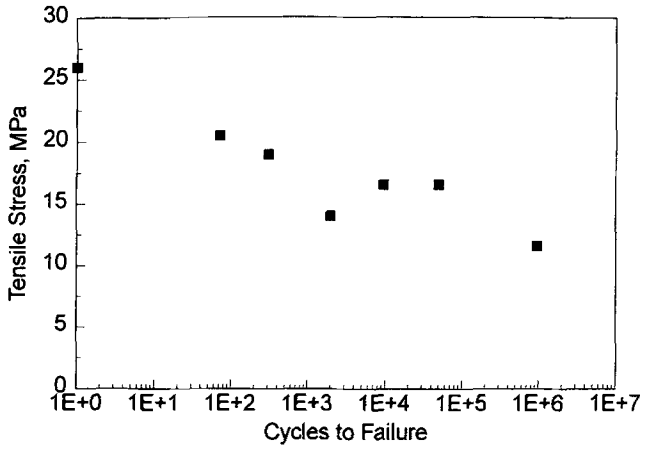


**Fig. 6** Tensile fatigue data generated using the modified axial test fixture (stress ratio=0)

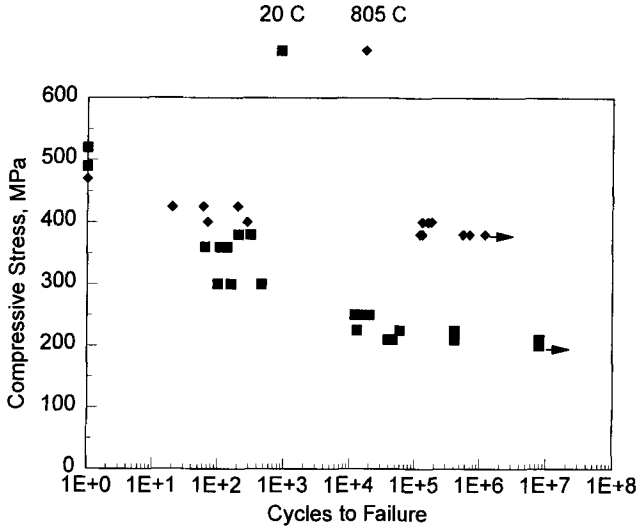


**Fig. 7** Comparison of room temperature and 800 °C test results for compressive fatigue strength of 8% yttria-zirconia

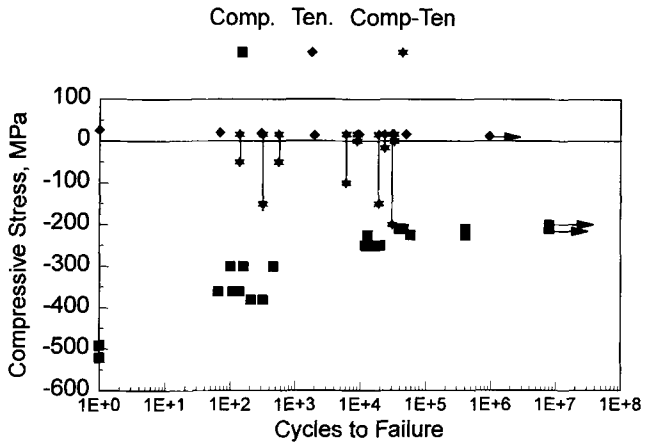


**Fig. 8** Comparison of the compressive, tensile, and combined compressive-tensile testing of an 8% yttria-zirconia TTBC

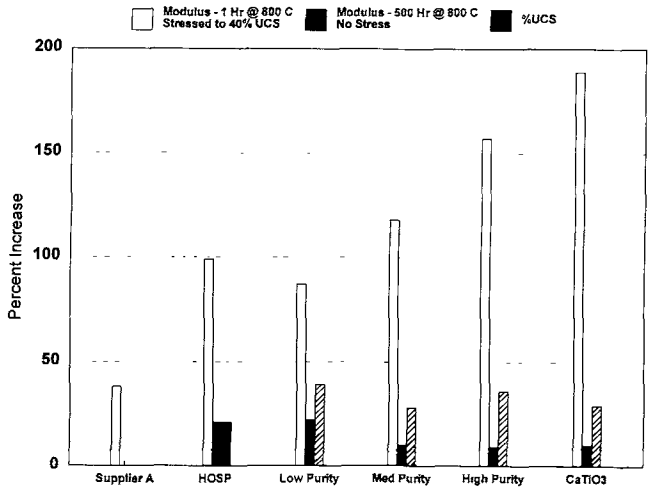


**Fig. 9** Increases in the elastic modulus and compressive strength of six of the materials in the aged condition (500 h, 800 °C, no load)

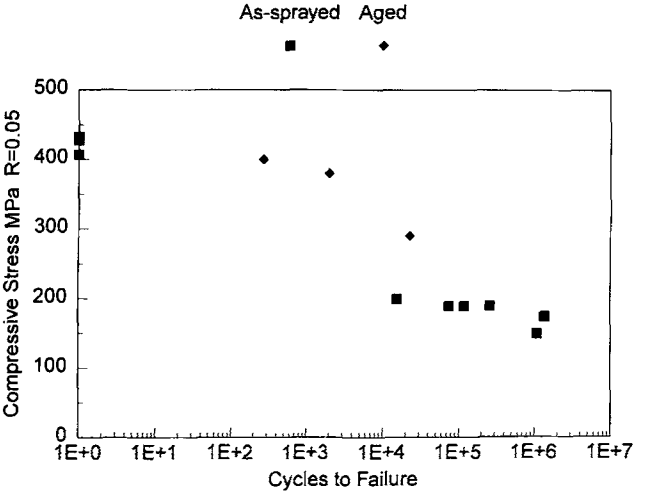


**Fig. 10** The fatigue strength of aged specimens (500 h, 800 °C, no load) and 8% yttria-zirconia baseline material (HOSP, lot A)

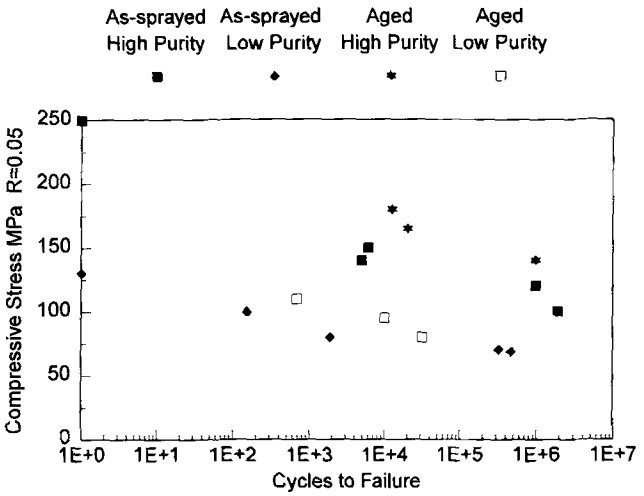


**Fig. 11** The fatigue strength of aged specimens (500 h, 800 °C, no load) for the high-purity (lot N) and low-purity (lot O) 8% yttria-zirconia

## 5. Aging Effects

The change in fatigue strength of the 8% yttria-zirconia at a high temperature indicates that properties of TTBC materials are not stable at high temperatures. To further investigate the change in the material properties with exposure at high temperatures, a furnace aging test was developed that uses a simulated diesel exhaust environment. This test exposes the specimens to 800 °C for 500 h, with no stress applied to the specimens. The resulting change in compressive strength and modulus of aged specimens for 6 of the 15 materials is compared to the change in modulus with the applied load in Fig. 9. The load applied was 40% of the compressive strength prior to aging. As shown in Fig. 9, the aging with no load at long intervals has a lesser effect than the stressed condition.

In addition to the static compressive strength and modulus measurements, fatigue studies on the furnace aged materials were also performed. As shown in Fig. 10 and 11, the fatigue strength of the aged specimens (500 h, 800 °C, no load) increased for all materials tested. The increase in the fatigue strength was not as large as for specimens held under load, but even the high-purity materials exhibited an increase in strength. A more detailed study of the stress-temperature time effects is needed to fully understand this phenomenon.

## 6. Conclusions

The effects of composition and manufacturing methods on TTBC powders and the resulting coating thermal conductivity and deposition efficiency was explored. The approach differs from past investigations because the spray parameters were optimized for each powder rather than using similar parameters. Methods to test the fatigue and aging behavior of the coatings have been developed and will be used in future investigations to develop life prediction models for the TTBC systems.

### Acknowledgments

Research was sponsored by the U.S. Department of Energy, Assistant Secretary for Conservation and Renewable Energy, and the Office of Transportation Technologies as part of the Ceramic Technology Project of the Materials Development Program, under contract DE-AC05-840R21400 with Martin Marietta Energy Systems, Inc.

### References

1. R.A. Miller, "Assessment of Fundamental Materials Needs for Thick Thermal Barrier Coatings (TTBC's) for Truck Diesel Engines," DOE/NASA/21749-1, NASA TM-103130, May 1990
2. M.B. Beardsley, "Thick Thermal Barrier Coatings," SAE P-278, *Proceedings of the Annual Automotive Technology Development Contractors' Coordination Meeting*, 1993, p 213
3. R.C. Brink, "Material Property Evaluation of Thick Thermal Barrier Coating Systems," 89-ICD-13, Energy Sources Technology Conference and Exhibition, The American Society of Mechanical Engineers, 1989
4. K.F. Wesling, D.F. Socie, and M.B. Beardsley, Fatigue of Thick Thermal Barrier Coatings, *J. Am. Ceram. Soc.*, Vol 77 (No. 7), 1994, p 1863-1868